Translational Oncology 14 (2021) 101099

Contents lists available at ScienceDirect

Translational Oncology

journal homepage: www.elsevier.com/locate/tranon

Original Research

Downregulation of PDGFRß Signaling Overcomes Crizotinib Resistance in a *TYRO3* and *ALK* Mutated Neuroendocrine-Like Tumor ☆

Colin H. Quinn[a], Andee M. Beierle[a], Adele P. Williams[a], Raoud Marayati[a], Laura V. Bownes[a], Hooper R. Markert[a], Jamie M. Aye[b], Jerry E. Stewart[a], Elizabeth Mroczek-Musulman[c], David K. Crossman[d], Karina J. Yoon[e], Elizabeth A. Beierle[a,*]

[a] *Division of Pediatric Surgery, Department of Surgery, University of Alabama at Birmingham, 1600 7th Ave. South, Lowder, Room 300, Birmingham, AL 35233, United States*
[b] *Division of Pediatric Hematology Oncology, Department of Pediatrics, University of Alabama at Birmingham, Birmingham, AL 35233, United States*
[c] *Department of Pathology, The Children's Hospital of Alabama, Birmingham, AL 35233, United States*
[d] *Department of Genetics, University of Alabama at Birmingham, Birmingham, AL 35233, United States*
[e] *Department of Pharmacology and Toxicology, University of Alabama at Birmingham, Birmingham, AL 35233, United States*

ARTICLE INFO

Keywords:
Targeted therapy
Drug resistance
Crizotinib
Neuroendocrine tumor
Patient derived xenoline

ABSTRACT

Patient-derived xenografts provide significant advantages over long-term passage cell lines when investigating efficacy of treatments for solid tumors. Our laboratory encountered a high-grade, metastatic, neuroendocrine-like tumor from a pediatric patient that presented with a unique genetic profile. In particular, mutations in *TYRO3* and *ALK* were identified. We established a human patient-derived xenoline (PDX) of this tumor for use in the current study. We investigated the effect of crizotinib, a chemotherapeutic known to effectively target both *TYRO3* and *ALK* mutations. Crizotinib effectively decreased viability, proliferation, growth, and the metastatic properties of the PDX tumor through downregulation of STAT3 signaling, but expression of PDGFRß was increased. Sunitinib is a small molecule inhibitor of PDGFRß and was studied in this PDX independently and in combination with crizotinib. Sunitinib alone decreased viability, proliferation, and growth *in vitro* and decreased tumor growth *in vivo*. In combination, sunitinib was able to overcome potential crizotinib-induced resistance through downregulation of ERK 1/2 activity and PDGFRß receptor expression; consequently, tumor growth was significantly decreased both *in vitro* and *in vivo*. Through the use of the PDX, it was possible to identify crizotinib as a less effective therapeutic for this tumor and suggest that targeting PDGFRß would be more effective. These findings may translate to other solid tumors that present with the same genetic mutations.

Introduction

Cancer is the leading cause of death by disease for children and a limited range of treatment options exists for this vulnerable patient population [1,2]. In the case of pediatric neuroendocrine cancers with unknown primaries, the survival rate is 10% [3]. Surgical excision is often the first step for treatment of pediatric solid tumors, followed by a regimen of chemotherapeutics and/or radiation therapy which are all associated with significant toxicities. Investigation of tumor mutations and signaling cascades is necessary to better target these malignancies and improve outcomes. It is also necessary to develop novel models to study these tumors to better understand the interaction between therapeutic agents and the tumor profile. The use of patient-derived xenolines (PDXs) makes this goal achievable. Tumor PDXs offer the unique opportunity to study both general cancer biology and the recapitulation of the tumor phenotype; conditions that provide an optimal opportunity to investigate and understand the potential effects of unexplored therapies prior to testing in a clinical setting [4].

Genomic sequencing of the PDX in this study identified mutations in anaplastic lymphoma kinase (*ALK)* and tyrosine kinase 3 *(TYRO3)* genes. In malignancies with *ALK* and/or *TYRO3* mutations, crizotinib, an ALK/c-Met-inhibitor, has been effective at decreasing tumor cell vi-

☆ **Financial support** This project was made possible by funding from the National Institute of Health under the 5T32GM008361 Medical Scientist Training Program (CHQ) and National Cancer Institute of the National Institutes of Health under award numbers, T32 CA229102 (RM and LVB), T32CA183926 (APW), CA013148 to the Genomics Core at the University of Alabama at Birmingham (UAB), and P30 AR048311 and P30 AI27667 to the Flow Cytometry Core at UAB. The content is solely the responsibility of the authors and does not necessarily represent the official views of the National Institutes of Health. Other funding sources include Sid Strong Foundation, Elaine Roberts Foundation, Open Hands Overflowing Hearts, and Starr Fund-Vince Lombardi Cancer Foundation (EAB).

* Corresponding author.
E-mail address: elizabeth.beierle@childrensal.org (E.A. Beierle).

https://doi.org/10.1016/j.tranon.2021.101099

ability, growth, and the metastatic properties in pre-clinical investigations [5-7]. Unfortunately, in the clinical setting, crizotinib has been less promising and efficacious. Multiple mechanisms of resistance have been proposed including upregulation of PDGFRß and Axl [8-11]. We hypothesized that similar mechanisms were in play in the PDX under current investigation, and that downregulation of PDGFRß utilizing sunitinib might overcome this drug resistance.

The complexity of molecular pathways in tumor cells may impede the ability to effectively treat patients, so understanding these pathways is critical for the successful development of new therapeutics. It is also crucial to appreciate the individual nature of each tumor and the differences amongst tumors, especially between adult and pediatric populations. The work presented addresses the ability to investigate a rare tumor on the molecular level and supports a mechanism of resistance while proposing a chemotherapeutic solution.

Methods

Establishing patient-derived xenoline

A high-grade neuroendocrine-like tumor from a pediatric patient who presented with multiple metastases was identified for potential use as a patient-derived xenograft, referred to as COA109 (Supplementary Figure 1 A). Following written informed consent and under an institutional review board approved protocol [University of Alabama at Birmingham (UAB) IRB 130627006], a fresh piece of the excised tumor was obtained from the surgical resection specimen and placed in iced Roswell Park Memorial Institute 1640 (RPMI) medium. The specimen was partitioned and placed in (i) formalin for paraffin embedding; (ii) liquid nitrogen for storage at −80 ˚C; and (iii) sterile media for implantation. Under a UAB institution animal care and use committee protocol, (IACUC 009186), implantation was accomplished using female athymic nude mice (Envigo, Prattville, AL). Briefly, animals were anesthetized with 3% inhalational isoflurane and under sterile conditions, 16 mm^3 tumor pieces were placed into the subcutaneous space of the animal's flank. Animals were housed in a pathogen-free environment and monitored for overall health and tumor growth. Tumor volumes were measured weekly and harvested when IACUC parameters were met. At the time of tumor harvest, the tumors were partitioned as described above, with the addition of a portion of the tumor being utilized for experimentation. For *in vitro* experiments, tumors were dissociated using a Tumor Dissociation Kit (Miltenyi Biotec, San Diego, CA) per manufacturer's protocol. Cells were resuspended in neurobasal (NB) medium (Life Technologies, Carlsbad, CA) supplemented with B-27 without Vitamin A (Life Technologies), N2 (Life Technologies), amphotericin B (250 μg/mL), gentamicin (50 μg/mL), L-glutamine (2 mM), epidermal growth factor (10 ng/mL, Miltenyi Biotec), and fibroblast growth factor (10 ng/mL, Miltenyi Biotec). Next-Generation Sequencing of COA109 xenograft tumor tissue and COA109 cells was completed (Genomics Core, UAB, Birmingham, AL) and results compared with FoundationOne® testing that had been completed on the patient's tumor to validate a similar tumor profile. Identified mutations were utilized for further testing. To ensure integrity of the PDXs through multiple passages, we performed short tandem repeat analysis (UAB Genomics Core, Birmingham, AL), real-time PCR (qPCR) to detect potential murine contamination of the PDX (TRENDD RNA/DNA Isolation and TaqMan QPCR/Genotyping Core Facility, UAB, Birmingham, AL), and histology and immunohistochemistry to confirm recapitulation of the patient's tumor.

Antibodies and reagents

The following antibodies were utilized per manufacturers' recommendations: rabbit monoclonal anti-phospho-Stat3 (Tyr705, D3A7, 9145), anti-Stat3 (79D7, 4904), anti-PARP (46D11), anti-Caspase-3 (9662), anti-cleaved Caspase 3 (Asp175, 5A1E, 9664), anti-Tyro3 (D38C6, 5585), anti-phospho-Akt (Ser473, D9E, 4060), anti-PDGFRβ (28E1, 3169), anti-Akt (11E7, 4685), anti-cyclin D1 (92G2, 2978), and anti-Vinculin (E1E9V, 13,901) from Cell Signaling (Danvers, MA); rabbit monoclonal anti-PDGF Receptor beta (Y92, ab32570) from Abcam (Cambridge, MA); mouse monoclonal β-actin (A1978), and anti-phospho-Erk 1/2 (AW39R) from Sigma Aldrich (Millipore Sigma, St. Louis, MO). Crizotinib was purchased from Sigma Aldrich and LC Laboratories (Woburn, MA) and sunitinib was purchased from Selleckchem (Houston, TX).

Immunohistochemistry

Paraffin-embedded COA109 tissue was cut into 4 μM sections onto positive slides and processed according to a previously published protocol [12]. Briefly, the primary antibody for Chromogranin A (ab15160, Abcam) was added at a 1:100 dilution and incubated overnight in a humidity chamber at 4 ˚C. The slides were then washed with PBS and secondary antibody for rabbit (R.T.U. biotinylated universal antibody, Vector Laboratories, Burlingame, CA) was added for 30 min at 22 ˚C. Staining reaction was applied for 30 min at room temperature with VECTASTAIN Elite ABC reagent (PK-7100, Vector Laboratories) and Metal Enhanced DAB Substrate (Thermo Fisher Scientific) for 2 min. Slides were counterstained with hematoxylin. Each antibody had a negative control (rabbit IgG, 1 μg/mL, EMD Millipore).

Immunoblotting

COA109 cells (1×10^6) were plated in non-adherent conditions in NB media and various drug treatments were applied for 24 h. Treated cell pellets were flash frozen in liquid nitrogen for later use. Whole cell lysates or homogenized tumor specimen lysates were made using either radioimmunoprecipitation (RIPA) buffer [10 mmol/L Tris base pH 7.2, 150 mmol/L NaCl, 1% Na-deoxycholate, 1% Triton X-100, 0.1% sodium dodecyl sulfate (SDS)] supplemented with phenyl-methanesulfonyl-fluoride (PMSF, Sigma), protease inhibitor (Sigma), and phosphatase inhibitor (Sigma), or mammalian target of rapamycin (mTOR) buffer [40 mM HEPES pH 7.5, 120 mM NaCl, 1 mM EDTA, 10 mM pyrophosphate (Sigma, P8010), 10 mM glycerophosphate (Sigma, G9891), 1.5 mM Na_3VO_4, 0.3% CHAPS, and EDTA-free protease inhibitors (Roche)] supplemented with protease inhibitor, 50 mM NaF, and PMSF according to protocols previously described [12]. Protein concentrations were determined with a Micro BCA Protein Assay Kit (Thermo Fisher Scientific, Waltham, MA). Proteins were separated on SDS polyacrylamide (SDS-PAGE) gels via electrophoresis. Precision Plus Protein Kaleidoscope molecular weight marker (Bio-Rad, Hercules, CA) was loaded adjacent to samples for reference. Gels were transferred to a blotting membrane using Trans-Blot Turbo Transfer System (Bio-Rad) per manufacturer's protocol. Antibodies were used per manufacturers' instructions. Blots were developed with either Immobilon Classico or Crescendo Western HRP Substrate (EMD Millipore, Millipore Sigma, Burlington, MA). Immunoblots were stripped with stripping buffer (Bio-Rad) at 65 ˚C for 20 min prior to re-probing. β-actin or vinculin were used to confirm equal protein loading.

Cell survival and proliferation

COA109 cells were suspended in Accutase (Fischer Scientific), incubated at 37 ˚C for 10 min, re-suspended in NB media, and counted. Cells (1.5×10^4) were plated in 96-well plates and treated with increasing doses of crizotinib (0, 0.5, 1, 2.5, 5, 10, 20 μm), sunitinib (0, 2.5, 5, 10 μm), or an equivalent concentration of dimethyl sulfoxide (DMSO) for a vehicle control. After 24, 48, and 72 h of treatment, an alamarBlue® colorimetric assay (Thermo Fisher Scientific) was used to assess viability. AlamarBlue® dye (10 μL, Thermo Fisher Scientific) was added and absorbance was read at 570 nm and 600 nm on a microplate reader (Epoch Microplate Spectrophotometer, BioTek Instruments, Winooski,

VT). To assess proliferation, cells (5×10^3) were plated in 96-well plates and treated with control, crizotinib, or sunitinib in increasing concentrations (as above) for 24, 48, and 72 h and the colorimetric CellTiter 96® Aqueous Non-Radioactive Cell Proliferation Assay (10 μL, Promega, Madison, WI) was utilized. Absorbance was read at 490 nm with a microplate reader. Cell viability and proliferation from at least three biologic replicates were reported as fold change ± standard error of the mean (SEM).

Cell growth

To assess *in vitro* cell growth over time, COA109 cells (5×10^5) were plated in non-adherent conditions and treated with control (DMSO) or crizotinib (1 μM) for single treatment studies. For combination studies, COA109 cells (2.5×10^5) were plated in non-adherent conditions and treated with control (0 μM), crizotinib (0.5 μM), sunitinib (0.5 μM), or a combination of crizotinib and sunitinib (0.5 μM each). Each time point (24, 48, 72, 96 h) had three wells of cells and all wells were treated at 0 h. Cells were brought to a single cell suspension, stained with trypan blue, and counted with a hemocytometer. Total cell population was compared across time points and presented with at least three biologic replicates.

Cell cycle

COA109 cells (5×10^5) were plated in 6-well plates with increasing doses of crizotinib (0, 2.5 μM). Following a 24-hour incubation period, cells were washed twice with PBS, fixed in ethanol for 24 h at 4 °C, stained with propidium iodide (1 mg/mL, Invitrogen), 0.1% TritonX (Active Motif, Carlsbad, CA), and RNAse A (0.1 mg/mL, Qiagen, Valencia, CA), and analyzed via Attune Next Su™ Flow Cytometer (Thermo Fisher Scientific). Collected data were analyzed using FlowJo software (Ashland, OR) and presented with at least three biologic replicates.

Migration and invasion

Corning® Transwell® plates (Corning Inc., Corning, NY) with 8 μm pore inserts were utilized. For both assays, the bottom of the inserts was coated with laminin (10 μg/mL, Millipore) overnight at 37 °C. Following treatment with increasing doses of crizotinib (0, 1, 2.5 μM) for 24 h, COA109 cells (2.5×10^5) were seeded into the inserts and allowed to migrate for 120 h. For invasion assays a similar method was used, but the top of the inserts was coated with Matrigel™ (1 mg/mL, 50 μL, BD Biosciences, Franklin Lakes, NJ) overnight at 37 °C. Following treatment with increasing doses of crizotinib (0, 1, 2.5 μM) for 24 h, COA109 cells (2.5×10^5) were seeded into the inserts and allowed to invade for 120 h. For both assays, inserts were fixed with 4% paraformaldehyde and stained with crystal violet. Image J (https://imagej.nih.gov/ij) was used for analysis and results were reported as fold change in number of cells migrating or invading ± SEM. Each assay had at least three biologic replicates.

In vivo *tumor studies*

PDX tumors were dissociated and cultured in NB media for 24 h. COA109 cells (5×10^6 in 25% Matrigel™, BD Biosciences) were implanted subcutaneously in the right flank of 6-week-old female athymic nude mice (Envigo). The mice were maintained in a pathogen-free environment with access to both chow and water *ad libitum* and under 12-hour light/dark cycles. Animals were monitored daily for overall body condition and weighed three times per week. Tumor volumes were measured three times a week with a caliper. Tumor volume was calculated with the formula ($\text{width}^2 \times \text{length}$)/2 with width being the smaller value.

Animals were randomized into two treatment groups for the single drug study: control (4% DMSO, $n = 7$) or crizotinib (75 mg/kg of body weight/day, $n = 7$, LC Laboratories). For drug combination studies, animals were randomized into four treatment groups: control (4% DMSO, $n = 5$), crizotinib (75 mg/kg of body weight/day, $n = 5$, LC Laboratories) [13], sunitinib (40 mg/kg of body weight/day $n = 5$, Selleckchem) [14], and crizotinib + sunitinib (same doses as single treatments, $n = 7$). Treatment was initiated one week after tumor cell implantation and was administered in a metronomic fashion: three consecutive days of each treatment with one day off per week. Drugs were delivered via oral gavage in 100 μL of corn oil and all animals received 100 μL of sterile saline subcutaneous injection daily for rehydration. The mice were treated for 17 days or until the tumors met IACUC parameters for animal euthanasia. Mice were humanely euthanized with CO_2 and cervical dislocation in their home cages one hour after their last treatment. Harvested tumors were saved for histologic sectioning and flash frozen for further experimentation.

Data analysis

Each *in vitro* experiment was repeated with at least three biologic replicates (PDXs from three different mice) and data was displayed as mean ± SEM. To determine statistical significance, a student's *t*-test or analysis of variance (ANOVA) was used as appropriate, with $p \leq 0.05$ determined to be statistically significant (SPSS V26, IBM®).

Results

Successful establishment of a high-grade pediatric neuroendocrine-like PDX

A high-grade pediatric neuroendocrine-like tumor, herein referred to as COA109, was successfully propagated as a PDX in immunodeficient mice. The PDX, COA109, was compared to the original patient tumor via histology. Hematoxylin and eosin staining demonstrated that the histology of the PDX (Fig. 1A, *top right panel*) recapitulated that of the parent tumor (Fig. 1A, *top left panel*). Both sections had round cells in a ribboning pattern and densely stained nucleoli (Fig. 1A, *top panels, black boxes*). Chromogranin-positive staining of the patient (Fig. 1A, *bottom left panel*) and PDX (Fig. 1A, *bottom right panel*) tumors suggested neuroendocrine features. IgG staining was included as a negative control (Fig. 1A, *insert, bottom right panel*). FoundationOne® sequencing was initially completed on the patient's tumor to identify mutations that might affect oncogenesis and to identify potential chemotherapeutic targets. FoundationOne® sequencing revealed mutations in 13 genes including *TYRO3* (Supplementary Figure 1 B). To confirm replication of the genotype of the parent tumor in the PDX, whole genome sequencing was performed on both COA109 dissociated cells that had been maintained in culture 24 h and directly from *ex vivo* tumor tissue. Next generation sequencing confirmed the alterations in *TYRO3* in the COA109 PDX tumors and cells from dissociated tumors, and detected mutations of unknown significance in *ALK*. There was over a 75% homology between *in vitro* and *ex vivo* samples, verifying the use of this PDX for experimentation (Supplementary Figure 1 C). Analysis showed all thirteen mutations identified by FoundationOne® were present in both the COA109 flank tumor and dissociated cells. These investigations validated a similar genotype between the PDX and the parent tumor. These findings supported the successful recapitulation of a rare tumor to be used for *in vitro* and *in vivo* studies as well as identified areas of investigation for therapeutics.

Crizotinib decreased viability, proliferation, growth, and cell invasiveness in vitro

ALK inhibitors have been studied in other tumors with *TYRO3* or *ALK* mutations, including non-small lung cancer [8,15,16], acute large cell lymphoma [17], leiomyosarcoma [7,18], and neuroblastoma [5,6]. Crizotinib is a rigorously researched ALK/c-Met-inhibitor. Based on its

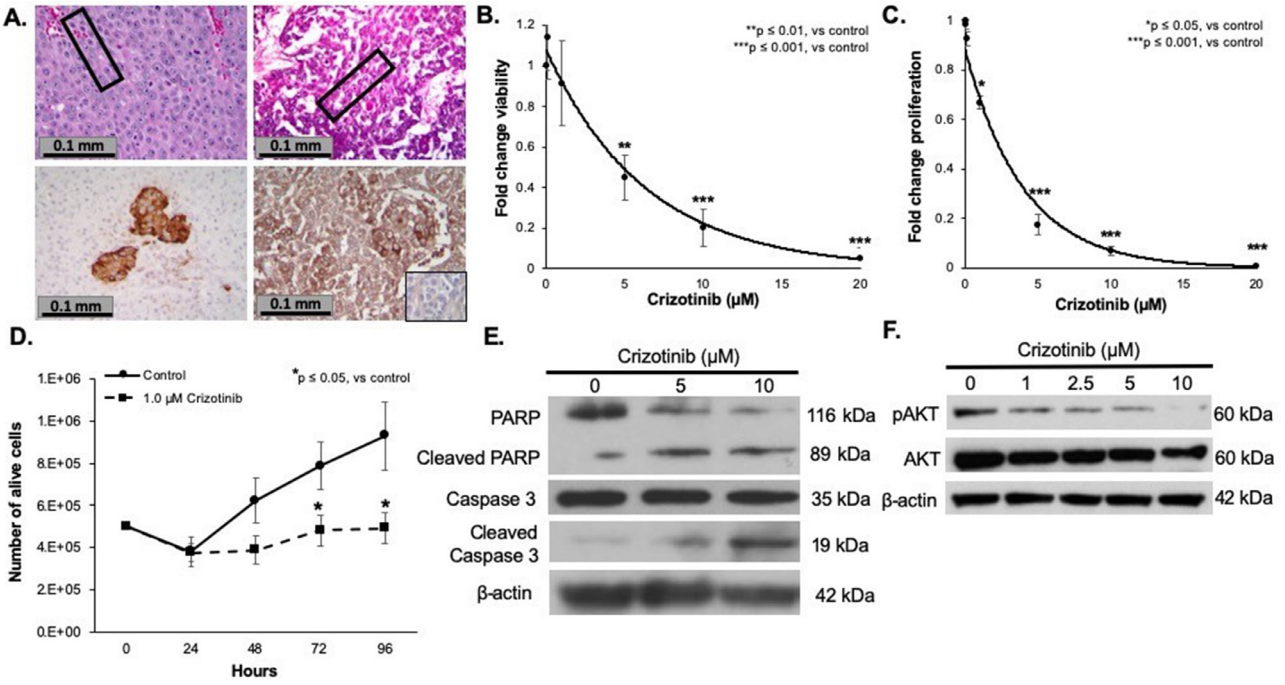

Fig. 1. Crizotinib decreased viability, proliferation, and growth in patient-derived xenoline cells of a highly malignant neuroendocrine tumor. A. Hematoxylin and eosin staining was performed on both the original patient tumor and the established PDX. Staining confirmed that the PDX morphology (*top right panel*) recapitulated that of the patient tumor (*top left panel*). Morphology of the tumor cells demonstrated densely stained nuclei and a gyriform-like pattern (*black boxes)*. Chromogranin A immunohistochemistry staining confirmed the neuroendocrine features in the PDX (*bottom right panel*) and patient (*bottom left panel*) tumors. IgG staining was included as a negative control (*insert, bottom right panel*). **B.** COA109 cells were treated with increasing doses of crizotinib (0 - 20 μM) for 24 h. Viability was assessed using an alamarBlue® assay. Viability was significantly decreased with increasing doses of crizotinib. Crizotinib had a measured LD_{50} of 4.87 μM. **C.** COA109 cells were treated with increasing doses of crizotinib (0 - 20 μM) for 24 h. Proliferation was evaluated using a CellTiter 96® assay. Proliferation was significantly decreased with increasing doses of crizotinib. Crizotinib had a measured IC_{50} of 2.24 μM. **D.** COA109 cells were treated with 1 μM of crizotinib and their growth was compared to a control group of COA109 cells over a 96-hour period. At 72 h, there was significantly less growth seen in COA109 cells treated with crizotinib. **E.** Immunoblotting showed an increase in both cleaved Caspase 3 and cleaved PARP, while there was a decrease in total PARP, indicating an upregulation of the apoptotic cascade. **F.** There was also a decrease in phosphorylation of AKT, consistent with decreased cell proliferation.

use in the pediatric population for neuroblastoma, another neuroendocrine tumor, the finding of alterations in *TYRO3* by FoundationOne®, and the discovery of mutations in *ALK* in the COA109 PDX and dissociated cells, we chose to investigate whether crizotinib would influence the phenotype of COA109 PDX cells. Dissociated PDX cells were treated with increasing concentrations of crizotinib (0 - 20 μM), and survival and proliferation were determined using alamarBlue® and CellTiter 96® assays, respectively. Crizotinib treatment led to a significant decrease in both viability and proliferation (Fig. 1B, C). Crizotinib was calculated to have a median lethal dose (LD_{50}) of 4.9 μM and half maximal inhibitory concentration (IC_{50}) of 2.2 μM. COA109 cell growth was assessed over a 96-hour period with 1 μM of crizotinib treatment. Starting at 72 h, cell growth was 39% less following treatment with crizotinib compared to COA109 cells under control conditions (Fig. 1D). Supporting apoptosis as the mechanism responsible for the associated cell death, there was an increase in the apoptotic markers, cleaved PARP and cleaved Caspase 3, and a decrease in total PARP with Crizotinib (Fig. 1E). Additionally, there was a decrease in phosphorylated AKT, explaining the decrease in cell proliferation (Fig. 1F).

Neuroendocrine tumors commonly metastasize [19] and research has demonstrated that Tyro3 may contribute to cancer cell motility [20]. We noted a decrease in Tyro3 expression with increasing doses of crizotinib (Fig. 2A), prompting us to examine cell migration and invasion. Modified Boyden chamber assays were used to evaluate migration and invasion. At increasing doses of crizotinib (0, 1, 2.5 μM), all below the LD_{50} to ensure independence from cell death, there was a significant decrease in both migration and invasion of COA109 cells (Fig. 2B). These data suggested that crizotinib led to decreased motility of COA109 cells.

To further delineate the possible mechanism responsible for crizotinib's effect on the survival and proliferation of COA109 cells, we investigated downstream signaling targets of Tyro3. We found a decrease in phosphorylation of STAT3 following treatment with crizotinib, suggesting a decrease in the activity of STAT3 (Fig. 2C). STAT3 regulates genes affecting cancer cell survival and proliferation, and inhibiting the function of STAT3 through de-phosphorylation at the TY705 site prevents the transcription of these oncogenes [21]. We propose that the results seen with crizotinib were due to alteration of the STAT3 signaling [18] as depicted in the cartoon (Fig. 2D).

Crizotinib did not affect in vivo *tumor growth*

Based on *in vitro* findings, the next step was to study crizotinib in an animal model. COA109 cells (5×10^6) were implanted into the right flank of female athymic nude mice. One week after injection, mice were randomized to receive either control [4% DMSO, 100 μL, *per os* (po), $n = 7$] or crizotinib (75 mg/kg, 100 μL, po, $n = 7$). The tumors were measured three times per week over a period of 37 days or until the mice reached IACUC parameters for euthanasia. Following 37 days of treatment, neither tumor volume (Fig. 3A, C) nor fold change in tumor volume (Fig. 3B) were significantly different between crizotinib and control animals. Additionally, crizotinib did not improve the survival of mice bearing COA109 tumors (Fig. 3D). These findings demonstrated the inability of crizotinib to decrease COA109 tumor growth and rate of tumor progression *in vivo* and posed the need to identify an alternative pathway that may be responsible.

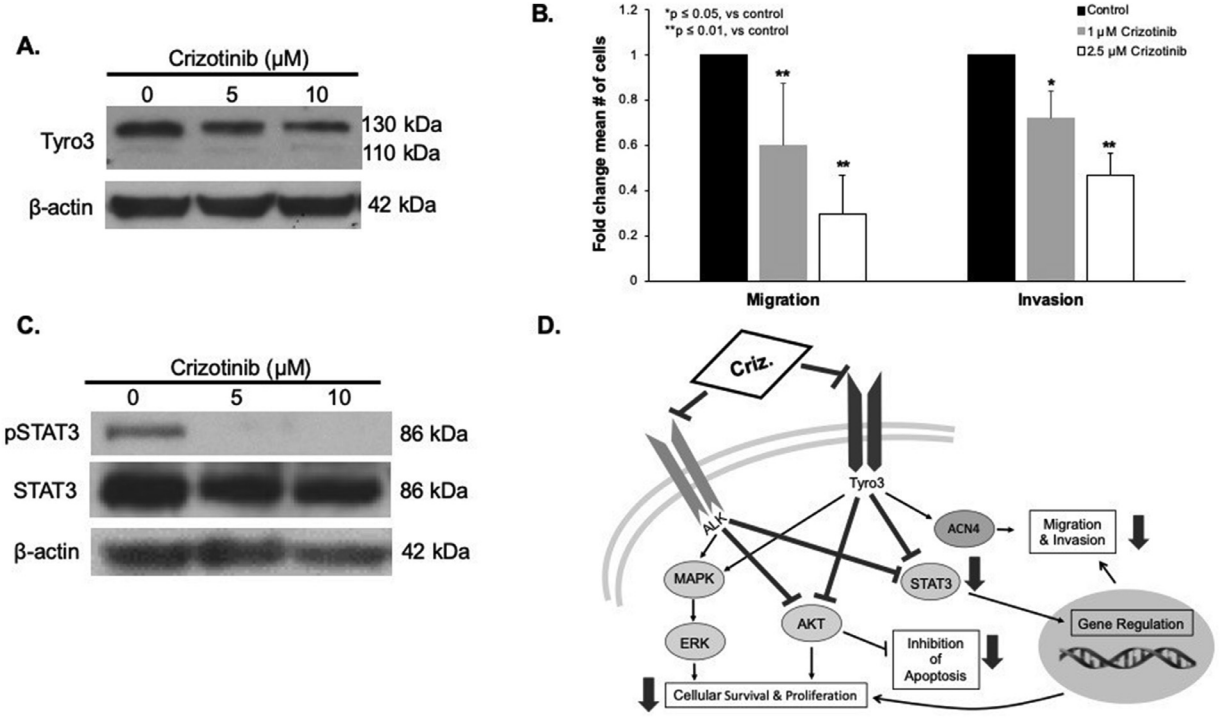

Fig. 2. Crizotinib treatment led to decreased Tyro3 and STAT3 activity. A. COA109 cells were treated with crizotinib (0, 5, 10 μM) for 24 h. Immunoblotting revealed a decrease in expression of Tyro3. **B**. Since Tyro3 affects cell motility, we studied migration and invasion using modified Boyden chambers. Following increasing doses of crizotinib, migration and invasion of COA109 cells was significantly decreased. **C**. STAT3 phosphorylation was evaluated with immunoblotting. There was a decrease in phosphorylated STAT3, indicating a downregulation of the JAK/STAT pathway. **D**. There is crosstalk between Tyro3 and ALK signaling cascades. This diagram represents a proposed mechanism.

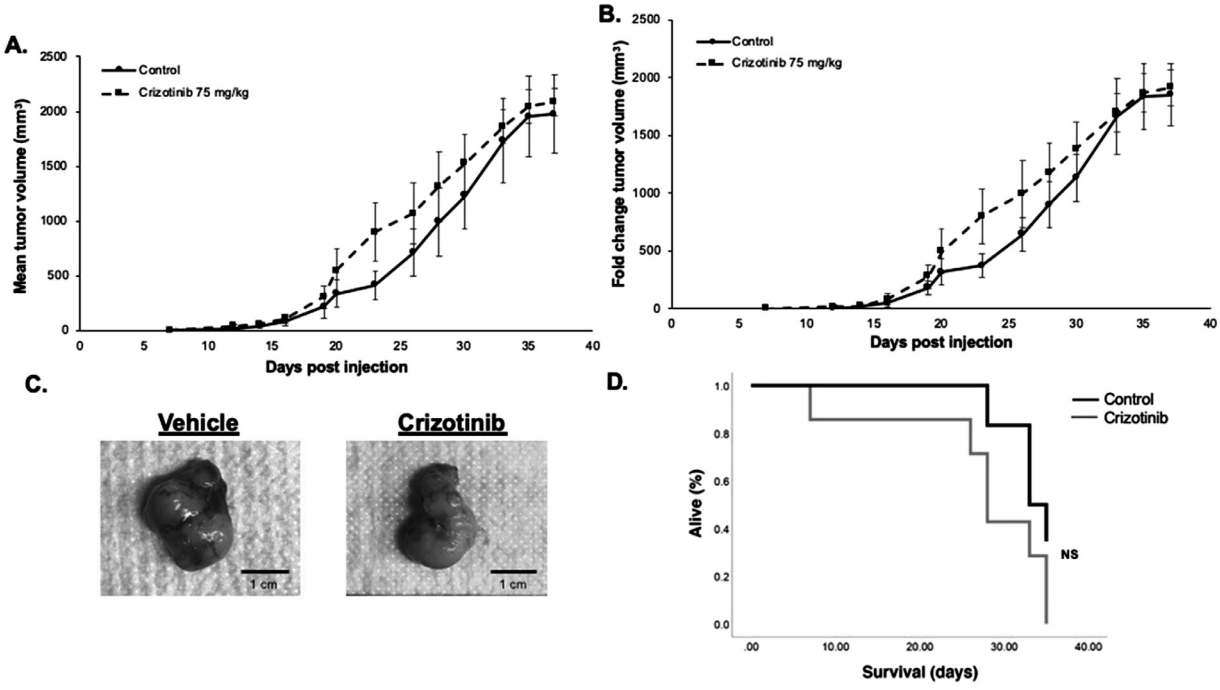

Fig. 3. Crizotinib did not decrease tumor growth *in vivo*. A-B. COA109 cells (5×10^6 in 25% Matrigel™) were placed subcutaneously in the right flank of athymic nude mice and tumor volume was measured three times a week and calculated as (width^2 × length)/2. One week after implantation, mice were treated with crizotinib (75 mg/kg, 100 μL, *per os,* $n = 7$) or control (4% DMSO, 100 μL, *per os,* $n = 7$). Mice treated with crizotinib had similar (**A**) tumor volume and (**B**) fold change in growth compared to the mice treated with control. **C.** Representative photos of excised tumors treated with control (*left*) and crizotinib (*right*). **D.** There was no statistically significant difference in survival between the control and crizotinib treated mice (NS, not significant).

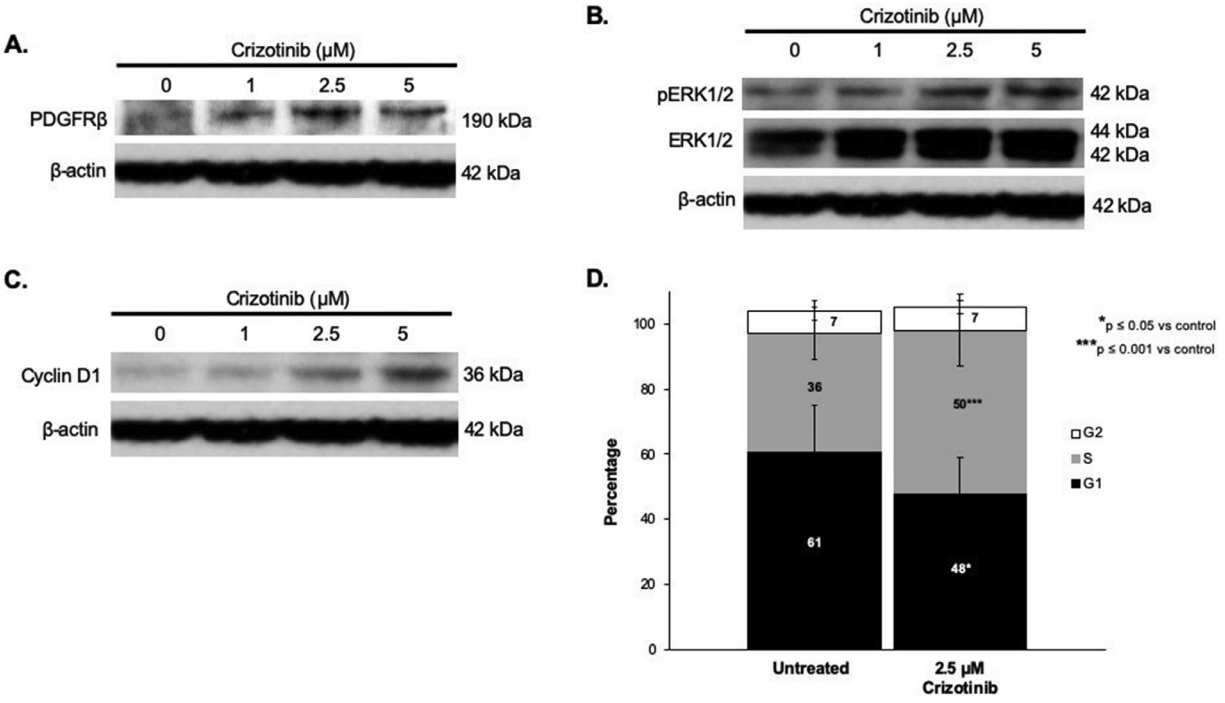

Fig. 4. PDGFR-β signaling was increased in crizotinib treated COA109 cells. Since crizotinib did not significantly affect *in vivo* tumor growth, potential mechanisms of resistance were investigated. **A.** COA109 cells (1×10^6) were treated with increasing doses of crizotinib (0 - 20 μM) and immunoblotting was performed on whole cell lysates. With increased doses of crizotinib, PDGFRβ expression was increased**. B.** There was increased phosphorylation of ERK1/2 after treatment with crizotinib, with no effect on total ERK1/2 expression. **C.** Downstream of PDGFRβ, there was also an increase in cyclin D1, a protein responsible for progression through the cell cycle from G1 to S phase. **D.** COA109 cells (5×10^5) were treated with crizotinib (0, 2.5 μM) for 24 h and examined via flow cytometry for cell cycle changes. With 2.5 μM of crizotinib, the percentage of cells in G1 phase significantly decreased while the percentage of cells in S phase significantly increased. The increase in cyclin D1 correlated with the observed effect noted with cell cycle analysis.

Increased PDGFRß in a crizotinib resistant cell subpopulation

Outcomes from the *in vivo* study contradicted those seen in the *in vitro* studies, prompting investigations for mechanisms to explain these findings. Other investigators have shown that malignancies treated with small molecule tyrosine kinase inhibitors have an upregulation of growth factors [22], and PDGFRß upregulation has been identified in some *ALK* mutation-driven cancers [10]. Since mutations in *ALK* were also noted in the COA109 PDXs we used immunoblotting to analyze COA109 cells treated with crizotinib for alterations in cell signaling. We noted that PDGFRß increased with increasing concentrations of crizotinib (Fig. 4A).

Due to the changes in PDGFRß, we chose to investigate downstream signaling cascades involved in tumor cell proliferation. There was an increase in phosphorylation of ERK 1/2 in COA109 cells treated with crizotinib (Fig. 4B). Consistent with increased ERK 1/2 activity, there was an increase in downstream cyclin D1 (Fig. 4C). The phosphorylation of ERK suggests that crizotinib causes some cancer cells to undergo proliferation while other cells, as previously shown, undergo apoptosis. We propose that this select subpopulation that was able to avoid cell death and proliferate may represent the cells responsible for the lack of efficacy seen *in vivo*.

Since we noted an increase in cyclin D1 following treatment with crizotinib, we investigated the cell cycle. Cyclin D1 is important for cell cycle progression from G1 phase to S phase. In cancer cells, halting this progression may prevent proliferation [23]. Using flow cytometry, cell cycle analysis was performed on COA109 cells treated with 2.5 μM of crizotinib. In control cells, 61% of the cell population was in G1 and 36% in S phase, while in the crizotinib-treated cells, 48% of cells were in G1 and 50% in S phase (Fig. 4D). The significant difference between G1 ($p<0.05$) and S ($p<0.001$) indicated cell cycle progression with crizotinib treatment. We then investigated the inhibition of upstream targets, such as PDGFRß, attempting to decrease the expansion of these resistant cells.

PDGFRß inhibition decreased COA109 survival and growth

Sunitinib is a small molecule tyrosine kinase inhibitor that effectively targets PDGFRß [24] and has been employed in clinical trials to treat pediatric malignancies [25]. Our data showed an upregulation of PDGFRß following crizotinib treatment and we hypothesized that by using sunitinib, we could counteract the increase in activity of proliferative kinases. To assess the effect of sunitinib on COA109 cells independently, an alamarBlue® assay was performed. Sunitinib significantly decreased viability of COA109 *in vitro* and had a calculated LD_{50} of 2.9 μM (Fig. 5A). These results provided substantiation to proceed with further experimentation of sunitinib alone and in combination with crizotinib.

Growth of COA109 cells over a 72-hour period was assessed under the following conditions: sunitinib + crizotinib (0.5 μM each), crizotinib (0.5 μM), sunitinib (0.5 μM), and control. At 48 h, sunitinib had a 24% and sunitinib + Crizotinib (combination) had a 36% decrease in growth compared to control ($p \leq 0.05$, $p \leq 0.01$, respectively). In comparing the combination group to each treatment alone, for crizotinib and sunitinib there were 32% and 38% and less cell growth at 72 h respectively ($p \leq 0.05$, $p \leq 0.01$, respectively, Fig. 5B). The findings for crizotinib were comparable with previous *in vitro* studies. These results suggested that combination treatment may be advantageous due to the cytotoxic effects of both drugs.

We then investigated the downstream mechanisms of crizotinib and sunitinib in combination. As previously shown, there was an increase in PDGFRβ expression and phosphorylation of ERK with increasing doses of crizotinib. At increasing doses of sunitinib alone, there was a decrease in phosphorylated ERK 1/2 (Fig. 5C), coinciding with the decrease in cell proliferation. Together, sunitinib in combination with crizotinib,

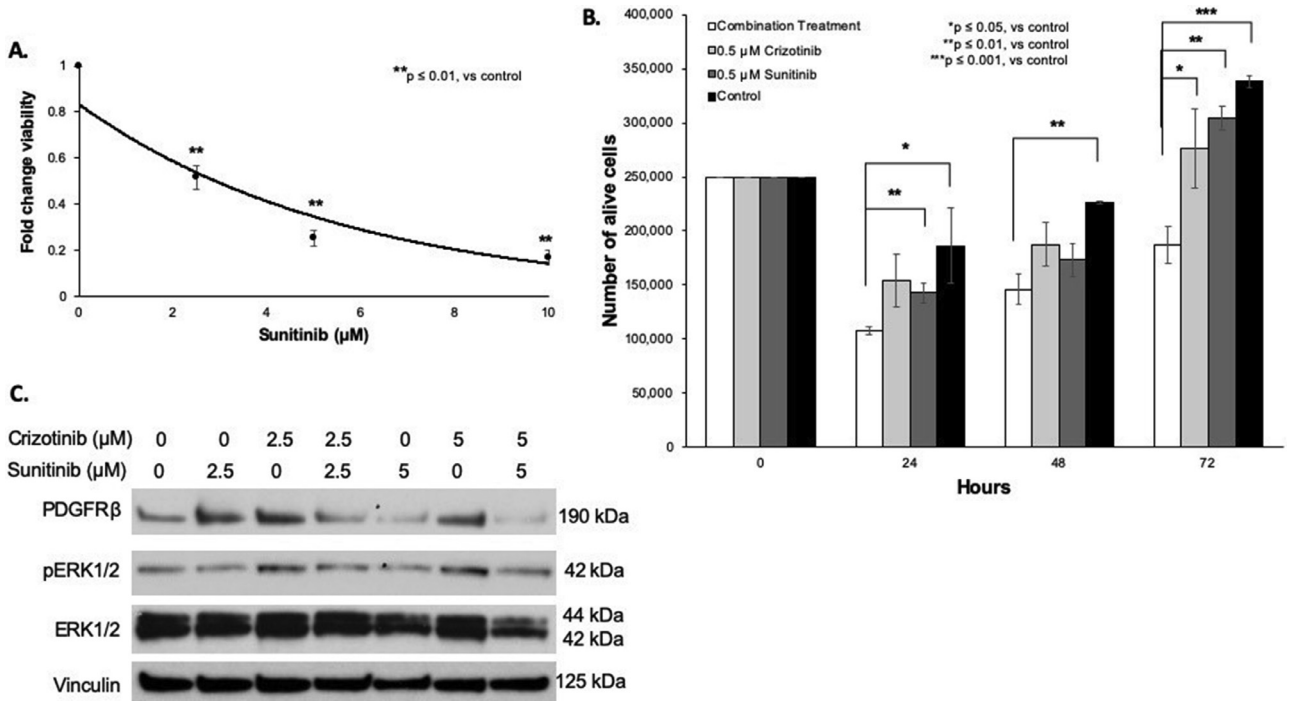

Fig. 5. Crizotinib and sunitinib in combination effectively targeted COA109 cells *in vitro*. A. COA109 cells were treated with increasing doses of sunitinib (0 - 10 μM) for 24 h. Using an alamarBlue® assay, viability was assessed and determined an LD_{50} of 2.9 μM. **B.** COA109 cells (2.5×10^6) were treated with a combination of 0.5 μM of crizotinib and 0.5 μM of sunitinib, 0.5 μM of sunitinib, 0.5 μM of crizotinib, or control. Cells were stained with trypan blue and counted at 24-hour intervals to assess growth over time. Combination treatment with crizotinib and sunitinib had the most significant inhibition on cell growth. **C.** Immunoblotting showed an increase in PDGFRβ and pERK 1/2 with crizotinib treatment, whereas there was no increase in pERK 1/2 with sunitinib treatment and a decrease in PDGFRβ with the addition of sunitinib.

decreased the expression of PDGFRβ (Fig. 5C), suggesting sunitinib was reducing the crizotinib-induced PDGFRβ upregulation. These results showed promise for the combined use of sunitinib with crizotinib *in vivo*.

PDGFRß inhibition decreased COA109 in vivo *tumor growth*

Because of the *in vitro* findings, we proceeded with studying sunitinib alone and in combination with crizotinib in a murine model. COA109 cells (5×10^6) were implanted subcutaneously in the right flank of athymic nude mice. At one week, animals were randomized to receive one of the following treatments: control (4% DMSO, 100 μL, po, $n = 5$), crizotinib (75 mg/kg of body weight/day, 100 μL, po, $n = 5$), sunitinib (40 mg/kg of body weight/day, 100 μL, po, $n = 5$), and crizotinib + sunitinib (same doses as in single treatments, 100 μL, po, $n = 7$). Animals were weighed and tumors measured three times per week for 20 days of treatment. Again, there was no significant difference between the tumor growth rate of the control treated group and those treated with crizotinib (Fig. 6A, B). Sunitinib alone significantly delayed COA109 tumor growth ($p \leq 0.001$, Fig. 6A, B). Further, the addition of sunitinib to crizotinib diminished tumor growth compared to the control ($p \leq 0.05$) and crizotinib treated groups, but not to sunitinib alone. These findings differed from the *in vitro* findings of combination treatment but substantiated the lack of efficacy of crizotinib *in vivo*.

Tumors from the experimental mice were harvested at euthanasia one hour after the final administration of treatment. Proteins were extracted from the tumors and immunoblotting completed. Consistent with our previous findings, tumors from mice treated with crizotinib (Fig. 6C) showed a high expression of PDGFRß and increased phosphorylation of ERK 1/2, indicating crizotinib had a similar effect on the *in vivo* tumor as it did *in vitro*. With the addition of sunitinib to crizotinib, PDGFRß and phosphorylation of ERK 1/2 were decreased (Fig. 6C). Sunitinib treatment alone decreased PDGFRß expression (Fig. 6C). These findings were consistent with the hypothesized mechanism of resistance to crizotinib mediated through PDGFRß signaling, and provide support for the use of sunitinib in tumors bearing this genotypic profile.

Discussion

Genetic mutations have become a driver for the development and use of targeted chemotherapeutics in cancer. We utilized the identified *TYRO3* and *ALK* mutations as a basis to study the use of crizotinib in an established PDX of a rare pediatric neuroendocrine-like tumor (Supplementary Figure 1 A-D). The *in vitro* data were promising with a decrease in COA109 cell viability, growth, and motility following treatment with crizotinib. When studied *in vivo*, crizotinib had little effect on the COA109 tumors, contradicting what was expected based on *in vitro* experiments. PDGFRß upregulation was noted with crizotinib treatment and suggested a potential resistance mechanism. Sunitinib was then added to override this activity and *in vitro* analysis suggested a potent combination for COA109. *In vivo* findings confirmed the lack of efficacy of crizotinib. Addition of sunitinib decreased *in vivo* tumor growth of the crizotinib resistant cells and on its own.

With the advent of genomic sequencing, it has become possible to pinpoint the specific, altered pro-oncogenic or pro-apoptotic signaling pathways in a cancer and target them for therapy. There are downfalls to this approach of personalized medicine: (i) the potential toxicity of these molecularly targeted therapies, and (ii) the inability of the targeted therapeutics to fully inhibit a protein's downstream activity [26]. Additionally, these pathways are subject to adaptability and may vary with the tumor microenvironment, providing an avenue for the development of drug resistance [16,27]. The use of PDX models allows for a more accurate prediction of a clinical outcome in a pre-clinical setting for chemotherapeutics as these models more closely replicate the properties of patient tumors [4]. A limitation to the PDX model is the amount of time required to grow the cancer in a murine model [28]. This barrier

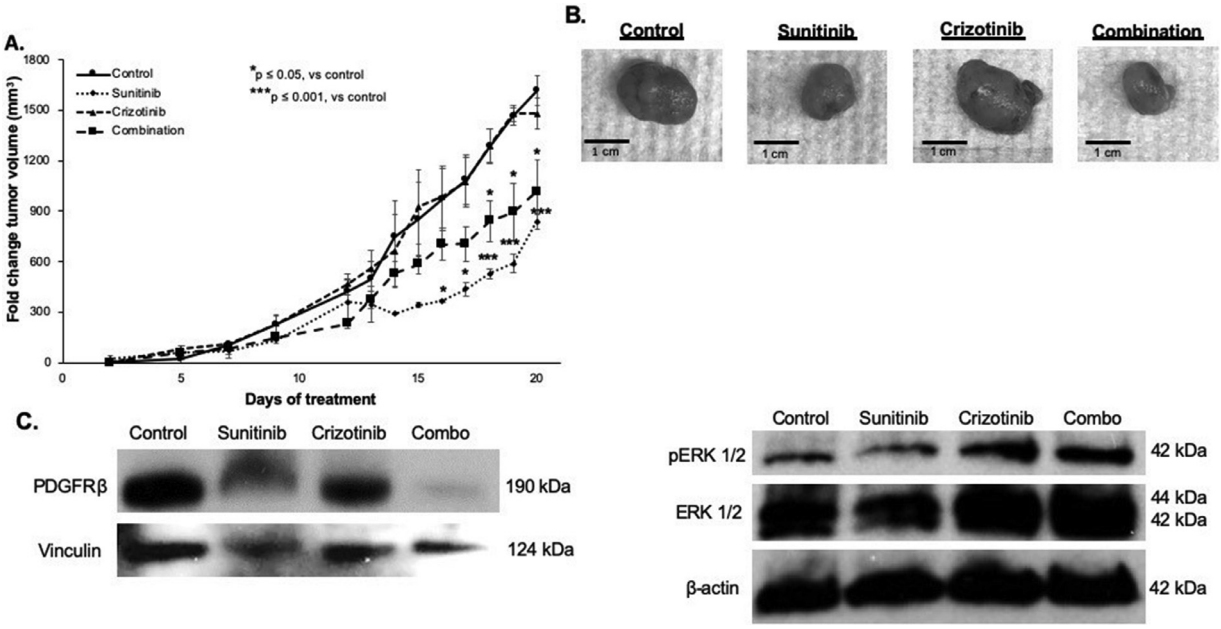

Fig. 6. Sunitinib significantly decreased tumor growth and improved crizotinib's affect *in vivo*. **A**. Athymic nude mice were implanted with COA109 cells (5×10^6) and randomized to four treatment groups: control (4% DMSO, 100 μL, *per os,* $n = 5$), sunitinib (40 mg/kg, 100 μL, *per os,* $n = 5$), crizotinib (75 mg/kg, 100 μL, *per os,* $n = 5$), or crizotinib + sunitinib (same as single doses, 100 μL, *per os,* $n = 7$). Fold change in tumor volume was decreased with sunitinib treatment alone and in the group receiving combined sunitinib and crizotinib treatment. As noted in previous experiments, crizotinib alone did not have an effect on tumor growth. **B.** Representative pictures of resected tumors of each treatment group are shown. **C.** Resected tumors were homogenized and lysed for immunoblotting. Tumors corroborated *in vitro* findings by demonstrating high levels of PDGFRß and increased phosphorylation of ERK 1/2 in crizotinib treated COA109 tumors. Both PDGFRß and phosphorylation of ERK 1/2 were lower in tumors treated with sunitinib or the combination of crizotinib + sunitinib.

was not encountered with the tumor in this study; COA109 tumors grew predictably within a month's time and at a similar rate with injection of dissociated cells, eliminating potential intertumoral selection bias that is associated with the implantation of tumor chunks. Other concerns with employing PDXs include genetic and phenotypic deviations of the PDX from the parent tumor after multiple passages; however, these were not encountered in this study. We showed that the COA109 PDX remained consistent with the original tumor through both histology and genotyping. The recapitulation of the parent tumor in a PDX model allowed for an in-depth study of the tumor's genotype and phenotype in order to better understand and explore potential therapeutic interventions.

The highly malignant features, variety of mutations, and lack of clear diagnostic pathology made this undifferentiated tumor challenging [29]. The focal neuroendocrine features were intriguing as there has been an increasing number of neuroendocrine tumors seen in adults but they remain rare in children [19]. Neuroendocrine tumors, however, are derived from the same embryonic tissue as the pediatric tumor, neuroblastoma, and led us to investigate potential similarities between COA109 and neuroblastoma. Identification of multiple *ALK* mutations in PDX tissue/cells served as a corroboration for initial studies (Supplementary Figure 2). ALK, an ATP-dependent tyrosine kinase receptor, is sparsely expressed throughout the body and is believed to play a role in neural development [30]. ALK signaling pathways have been found to be important for oncogenesis in neuroblastoma [31]. Up to 14% of high-risk neuroblastomas harbor *ALK* mutations and these mutations are known to promote oncogenesis through PI3K/AKT, RAS/MAPK, and STAT3 signaling pathways. F1774L, F1245C, and R175Q make up 85% of the *ALK* mutations found in neuroblastoma, but these specific mutations were not identified in the COA109 PDX. Additionally, in high-risk neuroblastoma, *ALK* mutations are often associated with *MYCN* amplification, the worst prognostic indicator in neuroblastoma, and *TP53* mutations [32,33]. The tumor in the current study had multiple *TP53* mutations but not *MYCN* amplification. Thus, the similarities between COA109 PDX and neuroblastoma were limited to sharing a neural ectoderm origin. Ultimately these findings eliminated neuroblastoma as the clinical diagnosis and led to the consideration of other neuroendocrine tumors for diagnosis.

Targeting ALK through tyrosine kinase inhibitors has been successful in *ALK* mutated malignancies. Crizotinib, a small molecule inhibitor of the ALK receptor, is an FDA approved drug that targets ALK fusion proteins and was initially developed for treatment of non-small cell lung cancer [34]. When studied in a PDX model of neuroblastoma, crizotinib did not significantly decrease *in vivo* tumor growth [35], similar to the findings presented in the current study. This resistance was attributed to the loss of TP53 function [35]. Studies have since showed a varying sensitivity of different *ALK* mutations to crizotinib, prompting investigations on the mechanisms of resistance or pathways to overcome resistance [5]. F1174L is the most widely known mutation to have *de novo* resistance to crizotinib and newer therapies such as lorlotinib have demonstrated improved efficacy over crizotinib in neuroblastoma lines with the F1174L mutation [13,36]. Even with these considerations, promising data with other long-term passage cell lines led to the initiation of a clinical trial. Recent reports of the study show less pronounced effects than anticipated and suggest the use of crizotinib for *ALK* mutations may not be as beneficial as anticipated (clinicaltrials.gov, NCT00939770). The discrepancy of crizotinib in pre-clinical findings compared to clinical use is similar to the contradiction we found in comparing our *in vitro* and *in vivo* results.

Crizotinib has been shown to inhibit other tyrosine kinase receptors such as TAM receptors [7,11]. The TAM receptor family is a group of tyrosine kinase receptors that includes Tyro3, Axl, and Mer [18]. Studies have shown the importance of TAM receptors in promoting cancer cell survival, metastasis, and chemoresistance through STAT3, PI3K/AKT, and RAS/MAPK pathways [11,18,37-40]. The PDX studied here had a *TYRO3* mutation (Supplementary Figure 1 C). Investigation of Tyro3 in other neural crest-derived malignancies has been focused on schwannoma and melanoma. Tyro3 has been shown to be overexpressed in schwannomas and activation of the receptor via Gas6 contributed to

an increased phosphorylation of ERK 1/2, AKT, and JNK, resulting in schwannoma cell proliferation [41]. In melanoma, Tyro3 activity decreased with focal adhesion kinase inhibition, which resulted in decreased metastases [20]. Finding that crizotinib successfully targeted Tyro3 in other neural crest-derived malignancies [42] prompted the use of crizotinib in these investigations. In *TYRO3*-mutated leiomyosarcoma, crizotinib was found to decrease tumor cell survival through inducing G2 cell cycle arrest and apoptosis [7]. Those findings were similar to those in the current studies where crizotinib decreased proliferation and increased apoptosis *in vitro* in the PDX studied but different in that crizotinib did not induce cell cycle arrest.

Coinciding downstream signaling of both ALK and Tyro3, such as PI3K/AKT, MAPK/ERK 1/2, and JAK/STAT, provides a promising area for targeted drug therapy [18,21,32,43,44]. Since the PDX in the current study had mutations in both *ALK* and *TYRO3*, it was hypothesized that crizotinib would be an effective agent. However, intercepting one signaling cascade over the other, or the inability to completely inhibit both, may result in the generation of a drug resistant tumor cell subpopulation [26]. This effect has been noted in *ALK* mutated neuroblastoma and non-small cell lung cancer. When these tumors were treated with ALK inhibitors, there was a subsequent increase in Axl receptor activity [9,45]. Specifically, increased Axl expression resulting from the *ELM4-ALK* fusion mutation induced resistance to ALK inhibitor in lung cancer. In the absence of *ALK* mutations and in pediatric solid tumors other than neuroblastoma, crizotinib has been shown to drive growth factor rescue and negate its therapeutic effects through upregulation of ERK 1/2 activity [22]. This finding could explain why PDGFRß expression is increased in *ALK*-mutated anaplastic large cell lymphoma (ALCL) which is resistant to crizotinib [10]. We showed both an upregulation of PDGFRß and activity of its downstream components including ERK 1/2 and cyclin D1 in COA109 following crizotinib treatment. Furthermore, we showed crizotinib-induced cell cycle progression, which may suggest proliferation of a crizotinib-resistant tumor cell subpopulation. We postulate that this cell subpopulation was responsible for the aberrant tumor growth seen *in vivo* in the crizotinib treated animals.

Inhibition of PDGFRß receptor signaling has also been investigated in *ALK*-mutated malignancies, as research has demonstrated that *ALK* mutations can increase transcription of its activator, JunB [8]. In ALCL, the inhibition of PDGFRß by iminatinib decreased tumor growth in mice bearing xenografts, and iminatinib's effects correlated with the levels of PDGFRß expression in the tumor. That study also demonstrated PDGFRß inhibition functioned in a synergistic fashion with crizotinib. It was effective at decreasing relapsed lymphoma growth, following an ALK inhibition relapse, when utilized in conjunction with CEP28122 (ALK inhibitor) [10]. Suntinib is another small molecule inhibitor of PDGFRß and has been shown to both decrease its phosphorylation and expression [46]. Sunitinib also has cytotoxic effects on neuroblastoma as well as off-target effects on Axl [14]. In medulloblastomas, similar to crizotinib, sunitinib decreased STAT3 activity as well as increased apoptosis [47]. Sunitinib also decreased AKT activity whereas crizotinib did not [47]. With this knowledge, we hypothesized that downregulation of PDGFRß may be a potential therapeutic option for this tumor. The *in vitro* results also suggested that sunitinib in combination with crizotinib functioned in an additive fashion, with *in vivo* studies demonstrating sunitinib to efficaciously decrease tumor growth independently and in combination with crizotinib.

Despite what our *in vitro* findings would suggest, combining crizotinib with sunitinib *in vivo* was not more effective than sunitinib alone. These findings could be explained by the contribution of the tumor microenvironment, which is absent *in vitro* studies. It is well documented the components of the tumor microenvironment, such as cancer associated fibroblasts and mesenchymal stromal cells, contribute to tumor progression, metastasis, and chemoresistance [48]. For example, in neuroblastoma, cancer associated fibroblasts can increase production of IL-6 [49] and it has been shown that IL-6 signaling leads to chemoresistance of common therapeutics like BCL2 inhibitors [49,50]. Clearly, utilizing models that include the tumor microenvironment, like patient-derived xenografts, are essential in pre-clinical drug testing.

This study only chose to investigate two of the many mutations identified in this tumor. Targeting both ALK and Tyro3 led us to expose mechanisms of resistance and understand the modest outcomes with crizotinib. Future studies will investigate the effects of sunitinib on the COA109 tumor profile. Additionally, there are other mutations with potential for chemotherapeutic targeting that may be explored. Although many of these treatments have targeted the adult population, translation to pediatrics could provide new therapeutic opportunities.

Conclusion

The establishment of a PDX of a rare, pediatric neuroendocrine-like tumor allowed for the exploration of tumor biology and the translation of the results into the investigation of targeted chemotherapeutics. In this study, the results of the *in vitro* studies using crizotinib were not replicated when tested *in vivo*, leading to the investigation of potential resistance mechanisms and the identification of PDGFRß signaling. We subsequently targeted PDGFRß to overcome this resistance. The current study has demonstrated some of the potential pitfalls to relying solely on genetic sequencing for treatment and highlighted the need for a more complete understanding of a drug's effect on a tumor, leading us to contend that caution should be exercised when employing crizotinib in *TYRO3/ALK* mutated malignancies.

Declaration of Competing Interest

The authors declare that they have no known competing financial interests or personal relationships that could have appeared to influence the work reported in this paper.

CRediT authorship contribution statement

Colin H. Quinn: Conceptualization, Methodology, Validation, Investigation, Visualization, Data curtion, Formal analysis, Writing – original draft, Writing – review & editing. **Andee M. Beierle:** Investigation, Formal analysis, Writing – review & editing. **Adele P. Williams:** Investigation, Formal analysis, Writing – review & editing. **Raoud Marayati:** Investigation, Writing – review & editing. **Laura V. Bownes:** Investigation, Formal analysis, Writing – review & editing. **Hooper R. Markert:** Investigation, Formal analysis, Writing – review & editing. **Jamie M. Aye:** Methodology, Resources, Writing – review & editing. **Jerry E. Stewart:** Investigation, Methodology. **Elizabeth Mroczek-Musulman:** Investigation, Validation, Visualization. **David K. Crossman:** Investigation, Formal analysis, Resources, Data curtion. **Karina J. Yoon:** Methodology, Resources. **Elizabeth A. Beierle:** Supervision, Conceptualization, Formal analysis, Writing – original draft, Writing – review & editing, Project administration, Funding acquisition, Resources.

Acknowledgments

The authors wish to thank Dr. Michael R. Crowley and the Genomics Core his assistance with the whole genome sequencing analysis. The authors also wish to thank Vidya Sagar Hanumanthu at UAB Comprehensive Flow Cytometry Core for his assistance.

Supplementary materials

Supplementary material associated with this article can be found, in the online version, at doi:10.1016/j.tranon.2021.101099.

References

[1] E. Ward, C. DeSantis, A. Robbins, B. Kohler, A. Jemal, Childhood and adolescent cancer statistics, 2014, CA Cancer J. Clin. 64 (2) (2014) 83–103, doi:10.3322/caac.21219.

[2] R.L. Siegel, K.D. Miller, A. Jemal, Cancer statistics, 2018, CA Cancer J. Clin. 68 (1) (2018) 7–30, doi:10.3322/caac.21442.

[3] P. Navalkele, M.S. O'Dorisio, T.M. O'Dorisio, G.K. Zamba, C.F Lynch, Incidence, survival, and prevalence of neuroendocrine tumors *versus* neuroblastoma in children and young adults: nine standard SEER registries, 1975-2006, Pediatr. Blood Cancer 56 (1) (2011) 50–57, doi:10.1002/pbc.22559.

[4] E. Izumchenko, K. Paz, D. Ciznadija, I. Sloma, A. Katz, D. Vasquez-Dunddel, et al., Patient-derived xenografts effectively capture responses to oncology therapy in a heterogeneous cohort of patients with solid tumors, Ann. Oncol. 28 (10) (2017) 2595–2605, doi:10.1093/annonc/mdx416.

[5] S.C. Bresler, D.A. Weiser, P.J. Huwe, J.H. Park, K. Krytska, H. Ryles, et al., ALK mutations confer differential oncogenic activation and sensitivity to ALK inhibition therapy in neuroblastoma, Cancer Cell 26 (5) (2014) 682–694, doi:10.1016/j.ccell.2014.09.019.

[6] E.L. Carpenter, Y.P. Mosse, Targeting ALK in neuroblastoma–preclinical and clinical advancements, Nat. Rev. Clin. Oncol. 9 (7) (2012) 391–399, doi:10.1038/nrclinonc.2012.72.

[7] C. Dantas-Barbosa, T. Lesluyes, F.L. Loarer, F. Chibon, I. Treilleux, J.M. Coindre, et al., Expression and role of TYRO3 and AXL as potential therapeutical targets in leiomyosarcoma, Br. J. Cancer 117 (12) (2017) 1787–1797, doi:10.1038/bjc.2017.354.

[8] A.S. Berghoff, P. Birner, B. Streubel, L. Kenner, M. Preusser, ALK gene aberrations and the JUN/JUNB/PDGFR axis in metastatic NSCLC, APMIS 122 (9) (2014) 867–872, doi:10.1111/apm.12249.

[9] D.N. Debruyne, N. Bhatnagar, B. Sharma, W. Luther, N.F. Moore, N.K. Cheung, et al., ALK inhibitor resistance in ALKF1174L-driven neuroblastoma is associated with AXL activation and induction of EMT, Oncogene 35 (28) (2016) 3681–3691, doi:10.1038/onc.2015.434.

[10] D. Laimer, H. Dolznig, K. Kollmann, P.W. Vesely, M. Schlederer, O. Merkel, et al., PDGFR blockade is a rational and effective therapy for NPM-ALK-driven lymphomas, Nat. Med. 18 (11) (2012) 1699–1704, doi:10.1038/nm.2966.

[11] F. Xu, H. Li, Y. Sun, Inhibition of Axl improves the targeted therapy against ALK-mutated neuroblastoma, Biochem. Biophys. Res. Commun. 454 (4) (2014) 566–571, doi:10.1016/j.bbrc.2014.10.126.

[12] L.L. Stafman, A.P. Williams, R. Marayati, J.M. Aye, H.R. Markert, E.F. Garner, et al., Focal adhesion kinase inhibition contributes to tumor cell survival and motility in neuroblastoma patient-derived xenografts, Sci Rep 9 (1) (2019) 1–12, doi:10.1038/s41598-019-49853-z.

[13] N.R. Infarinato, J.H. Park, K. Krytska, H.T. Ryles, R. Sano, K.M. Szigety, et al., The ALK/ROS1 inhibitor PF-06463922 overcomes primary resistance to crizotinib in ALK-driven neuroblastoma, Cancer Discov. 6 (1) (2016) 96–107, doi:10.1158/2159-8290.CD-15-1056.

[14] L. Zhang, K.M. Smith, A.L. Chong, D. Stempak, H. Yeger, P. Marrano, et al., *In vivo* antitumor and antimetastatic activity of Sunitinib in preclinical Neuroblastoma mouse model, Neoplasia 11 (5) (2009) 426–435, doi:10.1593/neo.09166.

[15] R. Katayama, A.T. Shaw, T.M. Khan, M. Mino-Kenudson, B.J. Solomon, B. Halmos, et al., Mechanisms of acquired crizotinib resistance in ALK-rearranged lung Cancers, Sci. Transl. Med. 4 (120) (2012) 120ra17, doi:10.1126/scitranslmed.3003316.

[16] T. Yamada, S. Takeuchi, J. Nakade, K. Kita, T. Nakagawa, S. Nanjo, et al., Paracrine receptor activation by microenvironment triggers bypass survival signals and ALK inhibitor resistance in EML4-ALK lung cancer cells, Clin. Cancer Res. 18 (13) (2012) 3592–3602, doi:10.1158/1078-0432.CCR-11-2972.

[17] P.B. Staber, P. Vesely, N. Haq, R.G. Ott, K. Funato, I. Bambach, et al., The oncoprotein NPM-ALK of anaplastic large-cell lymphoma induces JUNB transcription via ERK1/2 and JunB translation via mTOR signaling, BloodBlood 110 (9) (2007) 3374–3383, doi:10.1182/blood-2007-02-071258.

[18] S.K. Smart, E. Vasileiadi, X. Wang, D. DeRyckere, D.K. Graham, The emerging role of TYRO3 as a therapeutic target in cancer, Cancers (Basel) 10 (12) (2018) 1–27, doi:10.3390/cancers10120474.

[19] A.J. Degnan, S. Tocchio, W. Kurtom, S.S. Tadros, Pediatric neuroendocrine carcinoid tumors: management, pathology, and imaging findings in a pediatric referral center, Pediatr. Blood Cancer 64 (9) (2017), doi:10.1002/pbc.26477.

[20] H. Shao, A. Wang, D. Lauffenburger, A. Wells, Tyro3-mediated phosphorylation of ACTN4 at tyrosines is FAK-dependent and decreases susceptibility to cleavage by m-Calpain, Int. J. Biochem. Cell Biol. 95 (December 2017) (2018) 73–84, doi:10.1016/j.biocel.2017.12.014.

[21] J.S. Rawlings, K.M. Rosler, D.A. Harrison, The JAK/STAT signaling pathway, J. Cell. Sci. 117 (8) (2004) 1281–1283, doi:10.1242/jcs.00963.

[22] M. Sie, W.F.A. Den Dunnen, H.J. Lourens, T.G.J. Meeuwsen-De Boer, F.J.G. Scherpen, W.W. Zomerman, et al., Growth-factor-driven rescue to Receptor Tyrosine Kinase (RTK) inhibitors through Akt and Erk phosphorylation in pediatric low grade astrocytoma and ependymoma, PLoS ONE 10 (3) (2015) 1–16, doi:10.1371/journal.pone.0122555.

[23] S. Gookin, M. Min, H. Phadke, M. Chung, J. Moser, I. Miller, et al., A map of protein dynamics during cell-cycle progression and cell-cycle exit, PLoS Biol. 15 (9) (2017) e2003268 doi 10.1371/journal.pbio.2003268.

[24] A.I. Vinik, E. Raymond, Pancreatic neuroendocrine tumors: approach to treatment with focus on sunitinib, Therap. Adv. Gastroenterol. 6 (5) (2013) 396–411, doi:10.1177/1756283X13493878.

[25] S.G. Dubois, S. Shusterman, A.M. Ingle, C.H. Ahern, J.M. Reid, B. Wu, et al., Phase I and pharmacokinetic study of sunitinib in pediatric patients with refractory solid tumors: a children's oncology group study, Clin. Cancer Res. 17 (15) (2011) 5113–5122, doi:10.1158/1078-0432.CCR-11-0237.

[26] I.F. Tannock, J.A. Hickman, Limits to personalized cancer medicine, N. Engl. J. Med. 375 (13) (2016) 1289–1294, doi:10.1056/NEJMsb1607705.

[27] V. Davra, S.G. Kimani, D. Calianese, R.B. Birge, Ligand activation of TAM family receptors-implications for tumor biology and therapeutic response, Cancers (Basel) 8 (12) (2016), doi:10.3390/cancers8120107.

[28] N. Braekeveldt, D. Bexell, Patient-derived xenografts as preclinical neuroblastoma models, Cell Tissue Res. 372 (2) (2018) 233–243, doi:10.1007/s00441-017-2687-8.

[29] A. Hoppmann, A.P. Williams, A. Coleman, C. Tynes, G.R. Williams, E. Mroczek-Musulman, et al., Partial response to carboplatin, etoposide phosphate, and atezolizumab in a pediatric patient with high-grade metastatic tumor with rhabdoid and focal neuroendocrine features, Pediatr. Blood Cancer 67 (2) (2020) 7–9, doi:10.1002/pbc.28048.

[30] A. Cazes, L. Lopez-Delisle, K. Tsarovina, C. Pierre-Eugene, K. De Preter, M. Peuchmaur, et al., Activated Alk triggers prolonged neurogenesis and Ret upregulation providing a therapeutic target in ALK-mutated neuroblastoma, Oncotarget 5 (9) (2014) 2688–2702, doi:10.18632/oncotarget.1883.

[31] Y. Chen, J. Takita, Y.L. Choi, M. Kato, M. Ohira, M. Sanada, et al., Oncogenic mutations of ALK kinase in neuroblastoma, NatureNature 455 (7215) (2008) 971–974, doi:10.1038/nature07399.

[32] R.M. Trigg, S.D. Turner, ALK in neuroblastoma: biological and therapeutic implications, Cancers (Basel) 10 (4) (2018), doi:10.3390/cancers10040113.

[33] C. Schonherr, K. Ruuth, S. Kamaraj, C.L. Wang, H.L. Yang, V. Combaret, et al., Anaplastic lymphoma kinase (ALK) regulates initiation of transcription of MYCN in neuroblastoma cells, Oncogene 31 (50) (2012) 5193–5200, doi:10.1038/onc.2012.12.

[34] A.T. Shaw, D.W. Kim, K. Nakagawa, T. Seto, L. Crino, M.J. Ahn, et al., Crizotinib *versus* chemotherapy in advanced ALK-positive lung cancer, N. Engl. J. Med. 368 (25) (2013) 2385–2394, doi:10.1056/NEJMoa1214886.

[35] S. Durand, C. Pierre-Eug ne, O. Mirabeau, C. Louis-Brennetot, V. Combaret, L. Colmet-Daage, et al., ALK mutation dynamics and clonal evolution in a neuroblastoma model exhibiting two ALK mutations, Oncotarget 10 (48) (2019) 4937–4950, doi:10.18632/oncotarget.27119.

[36] J. Guan, E.R. Tucker, H. Wan, D. Chand, L.S. Danielson, K. Ruuth, et al., The ALK inhibitor PF-06463922 is effective as a single agent in neuroblastoma driven by expression of ALK and MYCN, Dis. Model. Mech. 9 (9) (2016) 941–952, doi:10.1242/dmm.024448.

[37] C.M. Gay, K. Balaji, L.A. Byers, Giving AXL the axe: targeting AXL in human malignancy, Br. J. Cancer 116 (4) (2017) 415–423, doi:10.1038/bjc.2016.428.

[38] F. Dufour, L. Silina, H. Neyret-Kahn, A. Moreno-Vega, C. Krucker, N. Karboul, et al., TYRO3 as a molecular target for growth inhibition and apoptosis induction in bladder cancer, Br. J. Cancer 120 (5) (2019) 555–564, doi:10.1038/s41416-019-0397-6.

[39] Y. Li, X. Wang, S. Bi, K. Zhao, C. Yu, Inhibition of Mer and Axl receptor tyrosine kinases leads to increased apoptosis and improved chemosensitivity in human neuroblastoma, Biochem. Biophys. Res. Commun. 457 (3) (2015) 461–466, doi:10.1016/j.bbrc.2015.01.017.

[40] C. Zhu, Y. Wei, X. Wei, AXL receptor tyrosine kinase as a promising anti-cancer approach: functions, molecular mechanisms and clinical applications, Mol. Cancer 18 (1) (2019), doi:10.1186/s12943-019-1090-3.

[41] S. Ammoun, L. Provenzano, L. Zhou, M. Barczyk, K. Evans, D.A. Hilton, et al., Axl/Gas6/NFκB signalling in schwannoma pathological proliferation, adhesion and survival, Oncogene 33 (3) (2014) 336–346, doi:10.1038/onc.2012.587.

[42] S.J. Demarest, J. Gardner, M.C. Vendel, E. Ailor, S. Szak, F. Huang, et al., Evaluation of Tyro3 expression, Gas6-mediated akt phosphorylation, and the impact of anti-Tyro3 antibodies in melanoma cell lines, Biochemistry 52 (18) (2013) 3102–3118, doi:10.1021/bi301588c.

[43] J.E. Brown, M. Krodel, M. Pazos, C. Lai, A.L. Prieto, Cross-phosphorylation, signaling and proliferative functions of the Tyro3 and Axl receptors in Rat2 cells, PLoS ONE 7 (5) (2012) 1–11, doi:10.1371/journal.pone.0036800.

[44] N.F. Moore, A.M. Azarova, N. Bhatnagar, K.N. Ross, L.E. Drake, S. Frumm, et al., Molecular rationale for the use of PI3K/AKT/mTOR pathway inhibitors in combination with crizotinib in ALK-mutated neuroblastoma, Oncotarget 5 (18) (2014) 8737–8749, doi:10.18632/oncotarget.2372.

[45] S. Nakamichi, M. Seike, A. Miyanaga, M. Chiba, F. Zou, A. Takahashi, et al., Overcoming drug-tolerant cancer cell subpopulations showing AXL activation and epithelial-mesenchymal transition is critical in conquering ALK-positive lung cancer, Oncotarget 9 (43) (2018) 27242–27255, doi:10.18632/oncotarget.25531.

[46] R.D. Spagnuolo, S. Brich, F. Bozzi, E. Conca, C. Castelli, M. Tazzari, et al., Sunitinib-induced morpho-functional changes and drug effectiveness in malignant solitary fibrous tumours, Oncotarget 7 (29) (2016) 45015–45026, doi:10.18632/oncotarget.7523.

[47] F. Yang, V. Jove, H. Xin, M. Hedvat, T.E. Van Meter, H. Yu, Sunitinib induces apoptosis and growth arrest of medulloblastoma tumor cells by inhibiting STAT3 and AKT signaling pathways, Mol. Cancer Res. 8 (1) (2010) 35–45, doi:10.1158/1541-7786.MCR-09-0220.

[48] L. Borriello, R. Nakata, M.A. Sheard, G.E. Fernandez, R. Sposto, J. Malvar, et al., Cancer-associated fibroblasts share characteristics and protumorigenic activity with mesenchymal stromal cells, Cancer Res. 77 (18) (2017) 5142–5157, doi:10.1158/0008-5472.CAN-16-2586.

[49] T. Kato, K. Noma, T. Ohara, H. Kashima, Y. Katsura, H. Sato, et al., Cancer-associated fibroblasts affect intratumoral CD8(+) and FoxP3(+) T Cells via IL6 in the tumor microenvironment, Clin. Cancer Res. 24 (19) (2018) 4820–4833, doi:10.1158/1078-0432.CCR-18-0205.

[50] T. Ara, R. Nakata, M.A. Sheard, H. Shimada, R. Buettner, S.G. Groshen, et al., Critical role of STAT3 in IL-6-mediated drug resistance in human neuroblastoma, Cancer Res. 73 (13) (2013) 3852–3864, doi:10.1158/0008-5472.CAN-12-2353.